Mechanical characterization of porous structures by the combined use of micro-CT and in-situ loading

G. Kerckhofs[1], J. Schrooten[1], L. Elicegui[1], S. Van Bael[2], M. Moesen[1], S.V. Lomov[1], M. Wevers[1]

[1] Dept. of Metallurgy and Materials Engineering, K.U.Leuven, Kasteelpark Arenberg 44 - bus 2450, B-3001 Leuven, greet.kerckhofs@mtm.kuleuven.be
[2] Dept. of Mechanical Engineering, Division of Production engineering, Machine design and Automation, K.U.Leuven, Celestijnenlaan 300b - bus 2420, B-3001 Leuven

Aims.

In order to understand and simulate the behaviour of porous materials during mechanical loading, a thorough knowledge of the relationship between their morphology and mechanical behaviour on the one hand, and the failure mechanisms on the other hand is required. Since most commonly used methods to characterize porous materials are either empirical, indirect, often destructive, or not normalized and thus not suitable for a reliable comparison, the combined use of microfocus X-ray computed tomography (micro-CT) and in-situ mechanical loading was proposed as a characterization technique to unravel the previously mentioned relationships [1-10]. This approach allows (i) to quantify the morphology prior and during loading, (ii) to determine in situ the global mechanical properties, (iii) to analyze the failure mechanisms and (iv) to quantify the internal local strain distributions [11-14]. The information thus obtained enables to link the morphology to the mechanical properties and failure mechanisms, and can serve as input or validation for Finite Element (FE) modelling and robust design.

In this study, the mechanical behaviour of porous Ti6Al4V structures produced by rapid prototyping with varying pore size and constant strut size was investigated via the combination of micro-CT imaging and stepwise in-situ compression. First the accuracy of the developed micro-CT loading stage was assessed by validation against a standard mechanical testing device. Then, the inter-batch variation of the morphology and mechanical properties was determined to check the robustness of the production technique, followed by a correlation between the morphology and the mechanical properties.

Materials and methods.

Materials.

Three different batches (n = 15) of cylindrical porous Ti6Al4V samples with regular structure and with varying pore and constant strut size were investigated (figure 1a). Table 1 summarizes their design parameters. They were produced by rapid prototyping (RP) and more specific by selective laser melting (SLM) [15, 16]. RP techniques [17-19] allow the production of porous materials that are based on a robust computer design, thus allowing a high morphological property control and hence eventually a wider use. All cylinders had a radius of 3.00 ± 0.05 mm and a height of 12.0 ± 0.5 mm. The design made use of unit cells, which can also be applied for FE modelling and determination of local surface strains as shown in figure 1b.

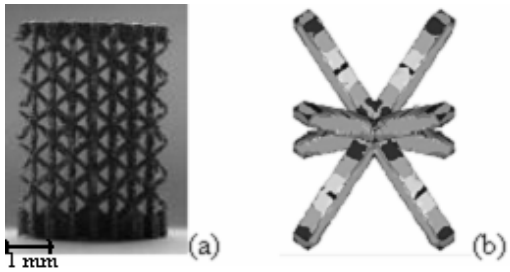

Figure 1. a) A typical cylindrical porous Ti6Al4V structure with a radius of 3.00 ± 0.05 mm, a height of 12.0 ± 0.5 mm and a global porosity of about 85 %. Designed pore size is 0.8 mm. (b) A typical unit cell of the designed porous structures. The differing grey values on the struts represent the surface strains under certain loading conditions.

Table. 1. Design parameters for the three different batches.

Batch	**Designed pore size (mm)**	**Designed strut size (mm)**	**n**
1	0.800	0.100	15
2	1.000	0.100	15
3	1.200	0.100	15

Micro-CT equipment

For this study, a Philips HOMX 161 X-ray system with AEA Tomohawk CT software was used. Characteristics of the device and the applied acquisition parameters can be found in Ref.[20]. In this study the thickness, width and height of the image voxels were 13.9 µm.

Mechanical loading devices

A mechanical loading stage was developed which can be installed inside a micro-CT device for in-situ measurements. This loading stage has the following advantages against others found in literature: (i) high forces can be attained (up to 30kN), (ii) monitoring and control of relaxation is possible, (iii) no tubing is present around the sample, thus low density polymers can be visualized accurately and (iv) there is a possibility to add a cooling/heating or an oxygen- and/or moisture-level regulated chamber. For standard mechanical testing, an INSTRON universal test bench, type 4505 equipped with an extensometer was used as reference. The compression rate was kept approximately the same on both loading devices, namely 0.15mm/min. On the INSTRON, a load cell of 5kN was used while the load cell on the micro-CT loading stage was 30kN.

Results and discussion.

Validation of the micro-CT loading stage against a standard mechanical testing device was performed on all three batches. Five samples per batch were continuously loaded on the INSTRON and five on the micro-CT loading stage. Since the designed porous structure shows non-linear elastic properties, the stiffness was defined as the maximum of the derivative of the stress-strain curve. Table 2 summarizes the results for stiffness, compressive strength and strain at maximum load. There was no significant difference between the results. This indicated that the micro-CT loading stage renders accurate and correct global mechanical properties.

Table 2. Stiffness, compressive strength and strain at maximum load determined both on the INSTRON and the micro-CT loading stage for five samples per batch.

	E-modulus (MPa)		**Strength (MPa)**		**Strain at maximum load (%)**	
Batch (n = 10)	**INSTRON**	**Micro-CT loading stage**	**INSTRON**	**Micro-CT loading stage**	**INSTRON**	**Micro-CT loading stage**
1	389.7 ± 22.6	369.8 ± 29.8	15.7 ± 0.3	14.8 ± 1.4	9.2 ± 0.5	7.3 ± 0.4
2	225.6 ± 20.5	237.7 ± 16.4	8.1 ± 0.3	8.0 ± 0.2	7.3 ± 0.2	7.2 ± 0.4
3	79.9 ± 5.2	81.9 ± 4.9	4.0± 0.09	3.9 ± 0.2	9.0 ± 0.6	8.2 ± 0.2

The combination of mechanical testing and micro-CT imaging allows to determine the morphological properties of each sample prior and during stepwise loading. In this way, a correlation can be made between the morphological and the mechanical properties. The analysed morphological properties based on the micro-CT datasets of all samples preloaded at 10N are summarized in table 3 together with physically measured properties.

Table 3. Morphological parameters derived via the Archimedes principle and from the micro-CT data via image analysis for the three different batches.

	Archimedes	**Micro-CT**				
Batch (n=5)	**Porosity (%)**	**Porosity (%)**	**Specific surface (1/mm)**	**Anisotropy**	**Avg. Pore size (µm)**	**Avg. Strut size (µm)**
1	85.3 ± 0.5	80.5 ± 1.1	21.9 ± 0.7	0.59 ± 0.02	480 ± 8	187 ± 5
2	88.1 ± 0.1	85.4 ± 0.3	21.6 ± 0.6	0.61 ± 0.02	601 ± 4	187 ± 4
3	92.2 ± 0.2	90.7 ± 1.1	22.8 ± 0.7	0.68 ± 0.10	776 ± 12	181 ± 5

It can be seen that the micro-CT based porosity values correspond well to those determined via the Archimedes principle, which serves as a physical reference [21, 22]. A small underestimation of the porosity is seen, which is mainly caused by the partial volume effect [20, 23, 24]. Table 3 also indicates that for each morphological parameter, the standard deviation within one batch is small. The same is seen in table 2 for the mechanical properties. This confirms the robustness of the production technique. Moreover, it indicates that one random sample within a batch is sufficient for a full batch characterization.

Additionally, table 3 confirms that the main difference between the three batches is the pore size and consequently also the specific surface and the porosity. It should be mentioned that the pore size in table 5 is an average value. In reality however, a distribution of pores with different diameter was found. The designed pore size and the one derived from the micro-CT data are defined differently and hence cannot be directly compared. For the struts also a distribution in diameter was found which was equal for the three batches. In the distribution curves, two peaks can be distinguished. The second peak, at larger strut size, represents the nodes in the unit cell (fig. 1b) and hence should not be accounted for as a strut. Therefore, a Gaussian curve was fitted to the first peak and the mean of this curve was taken as the average strut size of the structures. For the three batches, an average strut size of 178 ± 44 µm was found. Since the structures assessed in this study were designed close to the physical production limits, a difference between design (100 µm) and reality (178 µm) was expected.

Finally, as shown in figure 2, a correlation was found between stiffness and volume fraction determined via micro-CT. The exponential fit shows a factor 2.5. This factor indicates, as was expected, that the pore shape of the assessed structures lies between what Gibson and Ashby [25] define as being an open cell and a honeycomb. Equation 1 shows the correlation between the stiffness of the porous structure and the volume fraction for open cells. Thus, if open cells would be assumed, from the fit for the stiffness it could be concluded that the stiffness of the bulk rapid prototyped material should be about 47 GPa (fig. 4). This was indeed confirmed through experimental mechanical testing, showing an E-modulus for the bulk rapid prototyped Ti6Al4V of about 42 GPa.

$$E = E_s * (vol.frac.)^2 \qquad \text{eq. 1}$$

where E is the stiffness of the porous structure and E_s the stiffness of the bulk material [25].

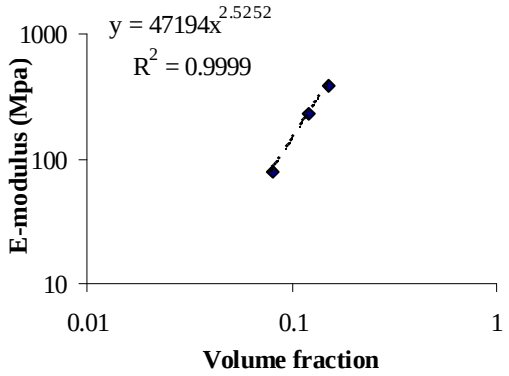

Figure 4. Correlation between the stiffness and the volume fraction of the samples, determined via micro-CT

Conclusion. The new micro-CT loading stage was proven to give accurate and correct results for the global mechanical properties of the tested rapid prototyped Ti6Al4V porous structures. It was also determined that there was no inter-batch variation for both morphological and mechanical properties. Thus, for further research, one random sample per design can be assessed as a representative. Finally, correlations between the morphology and the mechanical properties were made. The correlation functions can be applied to tailor the design according to the required stiffness and strength.

References.

1. Bart-Smith, H., et al., *Compressive deformation and yielding mechanisms in cellular Al alloys determined using X-ray tomography and surface strain mapping.* Acta Materialia, 1998. **46**(10): p. 3583-3592.
2. Maire, E., et al., *Recent results on 3D characterisation of microstructure and damage of metal matrix composites and a metallic foam using X-ray.* Materials Science and Engineering a-Structural Materials Properties Microstructure and Processing, 2001. **319**: p. 216-219.
3. Benouali, A.H., et al., *Investigation on the influence of cell shape anisotropy on the mechanical performance of closed cell aluminium foams using micro-computed tomography.* Journal of Materials Science, 2005. **40**(22): p. 5801-5811.
4. Dillard, T., et al., *3D quantitative image analysis of open-cell nickel foams under tension and compression loading using X-ray microtomography.* Philosophical Magazine, 2005. **85**(19): p. 2147-2175.
5. Toda, H., et al., *Quantitative assessment of microstructure and its effects on compression behavior of aluminum foams via high-resolution synchrotron X-ray tomography.* Metallurgical and Materials Transactions a-Physical Metallurgy and Materials Science, 2006. **37A**(4): p. 1211-1219.
6. Ohgaki, T., et al., *In situ observations of compressive behaviour of aluminium foams by local tomography using high-resolution X-rays.* Philosophical Magazine, 2006. **86**(28): p. 4417-4438.
7. Müller, R., S.C. Gerber, and W.C. Hayes, *Micro-compression: a novel technique for the nondestructive assessment of local bone failure.* Technology and Health Care, 1998. **6**: p. 433-444.
8. Nazarian, A. and R. Muller, *Time-lapsed microstructural imaging of bone failure behavior.* Journal of Biomechanics, 2004. **37**(1): p. 55-65.
9. Nazarian, A., M. Stauber, and R. Muller, *Design and implementation of a novel mechanical testing system for cellular solids.* Journal of Biomedical Materials Research Part B-Applied Biomaterials, 2005. **73B**(2): p. 400-411.
10. Nagaraja, S., T.L. Couse, and R.E. Guldberg, *Trabecular bone microdamage and microstructural stresses under uniaxial compression.* Journal of Biomechanics, 2005. **38**(4): p. 707-716.

11. Bay, B.K., et al., *Digital volume correlation: Three-dimensional strain mapping using X-ray tomography.* Experimental Mechanics, 1999. **39**(3): p. 217-226.
12. Roeder, B.A., et al., *Local, three-dimensional strain measurements within largely deformed extracellular matrix constructs.* Journal of Biomechanical Engineering-Transactions of the Asme, 2004. **126**(6): p. 699-708.
13. Smith, T.S., B.K. Bay, and M.M. Rashid, *Digital volume correlation including rotational degrees of freedom during minimization.* Experimental Mechanics, 2002. **42**(3): p. 272-278.
14. Wang, Y. and A.M. Cuitino, *Full-field measurements of heterogeneous deformation patterns on polymeric foams using digital image correlation.* International Journal of Solids and Structures, 2002. **39**(13-14): p. 3777-3796.
15. Snijkers, F., et al. *Porous Materials as Scaffold for Bone Replacement*. in *Acers-meeting*. 2005. Cocoa Beach, Florida, USA.
16. Impens, S., et al. *Production and characterization of CaP en Ti scaffolds for bone tissue engineering*. in *19th European Conference on Biomaterials*. 2005. Sorrento, Italy.
17. Leong, K.F., C.M. Cheah, and C.K. Chua, *Solid freeform fabrication of three-dimensional scaffolds for engineering replacement tissues and organs.* Biomaterials, 2003. **24**(13): p. 2363-2378.
18. Williams, J.M., et al., *Bone tissue engineering using polycaprolactone scaffolds fabricated via selective laser sintering.* Biomaterials, 2005. **26**(23): p. 4817-4827.
19. Hollander, D.A., et al., *Structural, mechanical and in vitro characterization of individually structured Ti-6Al-4V produced by direct laser forming.* Biomaterials, 2006. **27**(7): p. 955-963.
20. Kerckhofs, G., et al., *Validation of x-ray microfocus computed tomography as an imaging tool for porous structures.* Review of Scientific Instruments, 2008. **79**(1): p. -.
21. Ding, M., et al., *Age variations in the properties of human tibial trabecular bone.* Journal of Bone and Joint Surgery-British Volume, 1997. **79B**(6): p. 995-1002.
22. Ding, M., A. Odgaard, and I. Hvid, *Accuracy of cancellous bone volume fraction measured by micro-CT scanning.* Journal of Biomechanics, 1999. **32**(3): p. 323-326.
23. De Man, B., et al., *Metal streak artifacts in X-ray computed tomography: A simulation study.* Ieee Transactions on Nuclear Science, 1999. **46**(3): p. 691-696.
24. De Man, B., et al., *Reduction of metal streak artifacts in x-ray computed tomography using a transmission maximum a posteriori algorithm.* Ieee Transactions on Nuclear Science, 2000. **47**(3): p. 977-981.
25. Gibson, L.J. and M.F. Ashby, *Cellular solids: structure and properties*. 1988: Pergamon Press.